Nuclear Instruments and Methods in Physics Research A 1060 (2024) 169062

Contents lists available at ScienceDirect

Nuclear Inst. and Methods in Physics Research, A

journal homepage: www.elsevier.com/locate/nima

Characterization of bent crystals for beam collimation with 6.8 TeV proton beams at the LHC

Marco D'Andrea [a,*], Oliver Aberle [a], Andrey Abramov [a], Laura Bandiera [b], Roderik Bruce [a], Rongrong Cai [a,c], Marco Calviani [a], Quentin Demassieux [a], Kay Alana Dewhurst [a], Mario Di Castro [a], Luigi Salvatore Esposito [a], Yury Gavrikov [a], Simone Gilardoni [a], Vincenzo Guidi [b], Pascal Dominik Hermes [a], Yury Ivanov [a], Björn Hans Filip Lindström [a], Anton Lechner [a], Andrea Mazzolari [b], Eloise Matheson [a], Daniele Mirarchi [a], Jean-Baptiste Potoine [a,d], Stefano Redaelli [a], Gianmarco Ricci [a], Marco Romagnoni [b], Regis Seidenbinder [a], Santiago Solis Paiva [a], Melissa Tamisari [b]

[a] CERN, European Organization for Nuclear Research, CH-1211 Geneva 23, Switzerland
[b] INFN, Istituto Nazionale di Fisica Nucleare, Ferrara Division, Via Saragat 1, I 44122 Ferrara, Italy
[c] EPFL, École Polytechnique Fédérale de Lausanne, Route Cantonale, 1015 Lausanne, Switzerland
[d] University of Montpellier, 163 Rue Auguste Broussonnet, Montpellier, France

ARTICLE INFO

Keywords:
Crystal collimation
LHC
Proton beams

ABSTRACT

The concept of crystal collimation exploits the peculiar properties of crystalline materials to deflect high-energy beam particles at angles orders of magnitude larger than what can be achieved with scattering by conventional materials used as primary collimators. This innovative technique is planned to be used to improve the collimation efficiency with heavy-ion beams at the Large Hadron Collider (LHC) and its High-Luminosity upgrade (HL-LHC). The unprecedented proton-equivalent energy range of up to 7 TeV makes this technique particularly challenging due to the small angular acceptance of the crystal channeling process. This paper reviews the recent campaign of measurements performed with 6.8 TeV proton beams at the LHC to characterize the latest generation of crystal collimator devices installed in the machine, in preparation for the deployment in the upcoming heavy-ion runs.

1. Introduction

The Large Hadron Collider (LHC) [1], part of the accelerator complex of the European Organization for Nuclear Research (CERN), is designed to accelerate and collide two counter-rotating beams (Beam 1 clockwise and Beam 2 counterclockwise) of protons or heavy-ion nuclei. As part of the physics programme of Run 3 (2022–2025), a dedicated run with Pb ion beams will take place in October 2023 featuring the unprecedented energy of 6.8 Z TeV and 40% higher intensity compared to previous runs, as shown in Table 1 [2]. These higher intensity beams have been made available in the context of the LHC Injector Upgrade (LIU) [3] and High-Luminosity LHC (HL-LHC) [4,5] projects. Careful handling of beam losses is required to avoid quenching the superconductive magnets used to focus and bend the trajectory of the circulating beams [6].

The standard collimation system of the LHC [7], housed in dedicated Insertion Regions (IRs), provides multistage cleaning via a series of collimator families which progressively outscatter beam halo particles until they are lost in safe and controlled locations. In the case of ion beams, however, a large spectrum of secondary nuclei is generated in fragmentation and dissociation processes occurring at the collimators,

Table 1
Pb beam parameters at the start of collisions in the LHC as achieved in 2018 and as envisaged for Run 3 [2].

	2018	Run 3
Beam energy (Z TeV)	6.37	6.8
Total number of bunches	733	1240
Bunch spacing (ns)	75	50
Bunch intensity (10^7 Pb ions)	21	18
Stored beam energy (MJ)	12.9	19.9
Normalized transverse emittance (μm)	2.3	1.65

* Corresponding author.
E-mail address: marco.dandrea@cern.ch (M. D'Andrea).

https://doi.org/10.1016/j.nima.2023.169062
Received 27 October 2023; Received in revised form 15 December 2023; Accepted 24 December 2023
Available online 27 December 2023

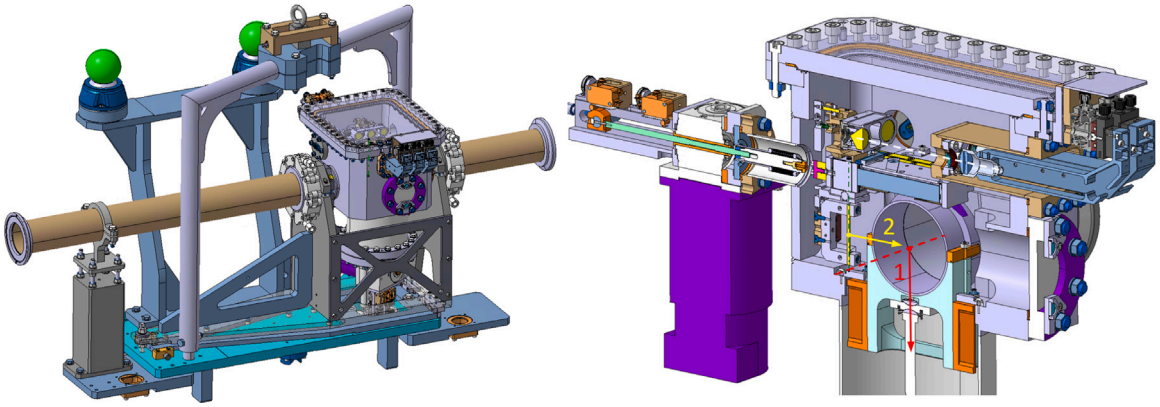

Fig. 1. Left: Schematic view of the full horizontal goniometer assembly installed on the LHC beam pipe. Right: Detail of the goniometer with its replacement chamber [9]. The direction of movement of the replacement chamber (1) and of the crystal (2) is shown.

in particular at the primary collimators of the betatron collimation system (located in IR7) [8]. Because of their different charge-to-mass ratio compared to the main beam, these fragments can escape the downstream collimation stages, generating losses at other locations around the ring. This results in a reduced collimation efficiency compared to proton beams. In particular a potential performance limitation was identified in the Dispersion Suppressor (DS) around the IR7 collimation insertion, where fragments generated in the collimators can induce magnet quenches.

To address these challenges, the innovative crystal collimation technique will be deployed for the first time in regular operation with high-intensity heavy-ion beams. The peculiar properties of crystalline materials, whose atoms are organized in a series of parallel planes, were studied at CERN for applications to beam extraction at the Super Proton Synchrotron (SPS) [10,11]. Applications to beam collimation were pioneered by the UA9 Collaboration and extensively validated at the CERN accelerator complex in recent years [12–15]. A positively charged particle with suitable impact conditions can get trapped in the potential well generated by adjacent planes and can travel through the crystal with a greatly reduced probability of inelastic interactions (*planar channeling*) [16]. A bent crystal can then be used to efficiently deflect beam halo particles without affecting the beam core [17], an effect that at the top energy of the LHC is equivalent to that of a magnetic field of hundreds of Tesla. Even with high-intensity ion beams, a standard secondary collimator can be safely used to intercept and dispose of the deflected halo [18].

This paper reviews measurements performed in Run 3 of the LHC with low-intensity proton beams at the unprecedented energy of 6.8 TeV with the goal of characterizing a new set of four devices, featuring newly produced crystals and an upgraded hardware assembly compared to previous installations. While the use of this technology in regular operation with proton beams (a factor 20 higher stored energy than ions) is hampered by the need to design a dedicated absorber capable of withstanding the channeled halo, these tests are extremely important to have early feedback on the devices in preparation of the ion run. Section 2 describes the crystal collimator devices presently installed at the LHC. Section 3 reports the result of the measurements performed with X-rays to validate the geometrical parameters of the crystals before their installation in the collimator assembly. The methodology and results of characterization measurements with proton beams at the LHC are described in Section 4. Finally, the main outcomes are summarized in Section 5.

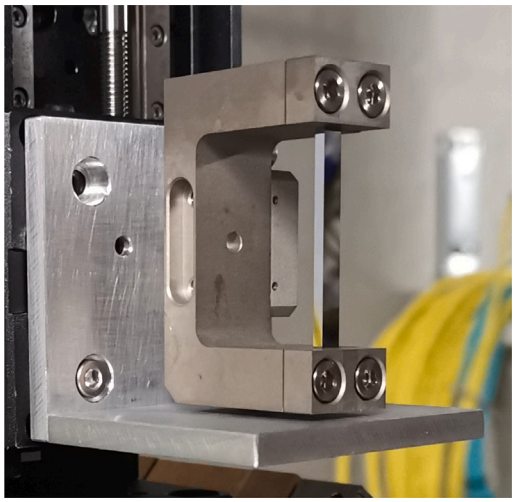

Fig. 2. Picture of a Si crystal clamped by its metal holder.

2. Crystal collimation hardware

The present crystal collimation setup of the LHC is comprised of a total of four devices, called Target Collimator Primary Crystals (TCPCs), one in the horizontal and one in the vertical cleaning plane of each beam [9]. A 3D model of the full assembly is shown in the left side of Fig. 1. Each device is composed of a metal holder that clamps a Si crystal (as shown in Fig. 2), in order to mechanically induce a secondary curvature of a specified bending of 50 μ rad over a length of 4 mm on the plane selected for particle steering. The holder is installed on a piezogoniometer which is used to measure and adjust the crystal orientation. The TCPC linear positioning control system is derived from that of the LHC collimation system, whereas the angular controls are based on a novel piezo-actuated rotational stage with interferometry feedback deployed for the first time in particle accelerators. The angular controls have a sub-μ rad precision. Such precision is required to achieve and maintain channeling conditions in the energy range of the LHC, where the angular acceptance of the channeling process is of the

Table 2
X-ray measurement of key crystal parameters: miscut, bending and torsion as measured before and after the bake-out (BO) cycles to 250 degrees Celsius used to validate equipment for ultra-high vacuum compatibility at the LHC. The uncertainty (Unc.) in the measurement accuracy achievable with the Panalytical machine setup is also reported.

Cleaning plane	Miscut (μrad)			Bending (μrad)			Torsion (μrad/mm)		
	Pre BO	Post BO	Unc. ±	Pre BO	Post BO	Unc. ±	Pre BO	Post BO	Unc. ±
B1H	1	1	2	54	51	2	−0.9	−0.9	1
B1V	6	5	2	47	49	2	−0.9	−1.1	1
B2H	3	3	2	49	47	2	0.2	0.5	1
B2V	3	3	2	52	52	2	0.6	0.1	1

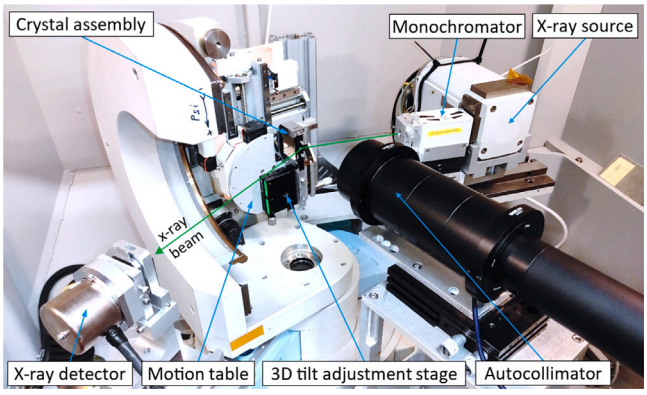

Fig. 3. Crystal and holder mounted in the Panalytical X'Pert Machine.

order of just a few μ rad. The TCPC assembly also includes a movable replacement chamber which hides the crystal from the circulating beam during standard proton operation, but can be moved out to allow the insertion of the crystal close to the beam. A schematic drawing of the goniometer is shown in the right side of Fig. 1. This design was conceived in order to minimize the impact on the impedance of the machine [19].

The first crystal collimation test stand was installed in the LHC during Run 2 [20–22], allowing the observation of the planar channeling process at multi-TeV energies for the very first time [14]. Compared to the original test stand, the latest generation of TCPCs developed internally at CERN for HL-LHC [9] and deployed already for Run 3 of the LHC, features a number of upgrades aimed at improving the stability and reproducibility of the devices in long-term operation. In particular, the interferometric heads of the crystal orientation readout system were moved outside the vacuum chamber, allowing maintenance of optical components without the need to open the vacuum tank, and reducing the risk of radiation damage that could impact the working range of the goniometer.

3. Validation of crystal parameters with X-rays

X-ray Bragg diffraction can be used to measure and precisely characterize key geometrical parameters of bent crystals, by accessing information on the orientation of the lattice planes. X-rays have wavelengths of similar size to the spacing between atoms within the crystal lattice and by using crystal diffraction based on Bragg's law it is possible to understand how the orientation of the planes behaves across the structure of the crystal. As a result, the bending angle, torsion (associated with a twist effect created by the holder) and miscut angle (defined as the angle between the crystalline planes and the crystal surface) can be measured. Particularly relevant is the measurement of the miscut, which was found in simulation to have an effect on the expected LHC cleaning performance [23]. This information is not accessible through measurements with hadron beams that are typically performed in the CERN-SPS North Area facilities [24,25]. Through different X-ray measurements across the crystal surface, several scans are performed in order to obtain a map of the Bragg peak from a lattice plane. The bending angle and miscut angle are then calculated by analyzing the shift of the angular peak over the width of the crystal. Similarly, the torsion is obtained by extending the analysis to the height of the crystal. The parameters of bending and torsion are also accessible in hadron-beam tests [26], however such tests are complex and resource-demanding. The possibility to perform a pre-selection of the crystals through a complete X-ray characterization is an important asset for the identification of the best candidates to be also tested with hadron beams. To be noted that the X-ray validation process is repeated after a standard bake-out (BO) applied to the LHC equipment to 250 degrees Celsius, to ensure the long term stability of the crystal and holder. It is important to recall that tests with hadron beams are nevertheless a crucial part of the crystal characterization and validation procedure, as they provide the unique opportunity to measure the single-pass efficiency of the channeling process before installation in the LHC. More details on the experimental and analysis procedure of these measurements can be found in [25,26].

A Panalytical X'Pert X-ray diffractometer [27], see Fig. 3, combined with a custom autocollimator for crystal angular orientation feedback, was used to perform the measurements, resulting in the values and uncertainty in measurements given in Table 2.

4. Characterization measurements with proton beams at the LHC

Characterization measurements were carried out with low-intensity proton beams at the injection energy of 450 GeV and at the top energy of 6.8 TeV, following the well established procedures defined in previous tests at the SPS and at the LHC [13–15,28,29]. Data for these measurements are collected via the Beam Loss Monitoring (BLM) system [30], which consists of more than 3900 ionization chambers placed around the accelerator ring at likely or critical loss locations to detect products of nuclear interactions of beam particles with machine elements. Due to the physics of the interaction processes at play, crystal collimation produces peculiar loss patterns that allow measuring the geometrical properties and channeling efficiency of a crystal device.

After the replacement chamber of each TCPC is moved out, the crystals are inserted towards the beam using a *beam based alignment* procedure similar to what is done for standard collimators [31]. Each crystal is moved until the corresponding BLM detects a sudden loss spike, signaling that the primary beam halo has been touched and thus the crystal has become the primary bottleneck of the ring. After this first step is completed, all collimators upstream of the crystal and all secondaries located between the crystal and the corresponding absorber of the channeled halo, are retracted. This is done to remove other elements that can generate particle showers and thus have cleaner BLM signals at the location of the crystal and of the absorber. Additionally, primary beam losses on the collimation system are increased by

Table 3
Measured crystal parameters with proton beams at injection and at top energy. Due to time constraints, no measurements could be performed with the Beam 1 horizontal crystal at top energy.

Cleaning plane	450 GeV		6.8 TeV	
	Bending angle [μrad]	Channeling efficiency	Bending angle [μrad]	Channeling efficiency
B1H	47.5 ± 2.5	82 ± 15%	n.a.	n.a.
B1V	45.2 ± 2.3	75 ± 26%	47.4 ± 2.4	68 ± 17%
B2H	47.1 ± 2.4	86 ± 18%	45.4 ± 2.3	70 ± 11%
B2V	52.1 ± 2.5	87 ± 19%	49.1 ± 2.5	73 ± 21%

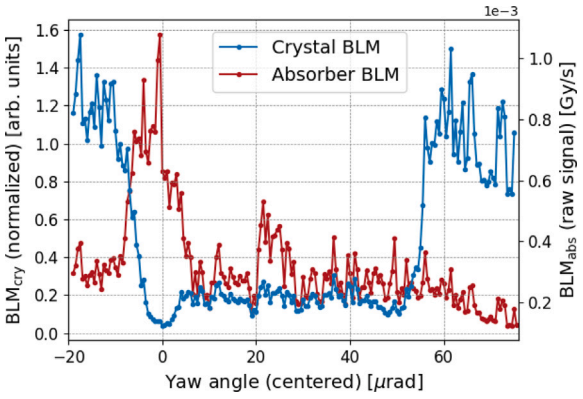

Fig. 4. Normalized BLM signal measured at the crystal location during an angular scan (vertical crystal, Beam 1) with proton beams at 6.8 TeV. The raw BLM signal measured at the absorber location is also shown.

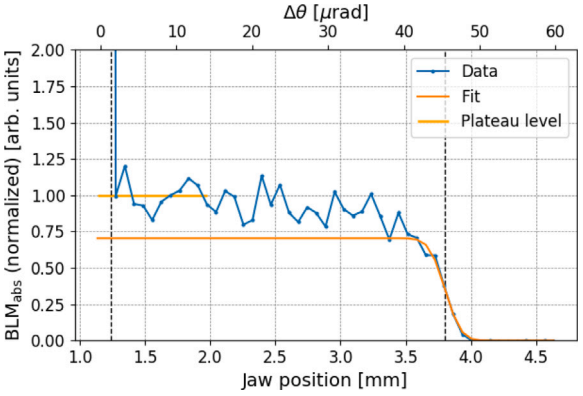

Fig. 5. Normalized BLM signal measured at the absorber location during a linear scan (horizontal crystal, Beam 2) with proton beams at 6.8 TeV. The position of the absorber jaw is measured from the beam axis. The error function fit on data and the plateau of the measured profile are also shown. The vertical dashed lines indicate the estimated location of the beam envelope (left side) and of the center of the channeled beam (right side).

using the Transverse Damper (ADT) to induce a controlled emittance blow-up. In these conditions, two types of measurements are then performed [29].

During an *angular scan*, the aligned crystal collimator is rotated at constant speed along the deflection plane. The probability of different interaction processes between halo particles and the crystalline lattice changes with the relative orientation of the crystal with respect to the beam halo. During this movement, a peculiar behavior is observed in the signal recorded by the BLMs located close to the crystal and downstream absorber. When the crystal is in the orientation that maximizes the probability of channeling, and thus minimizes the probability of inelastic interactions with the atoms of the crystalline lattice, losses recorded at the location of the crystal are reduced. Conversely, losses at the location of the absorber increase as more and more halo particles are deflected towards it. This characteristic pattern identifies the optimal channeling orientation, to be used as a reference for long-term use in operation. An example measurement is shown in Fig. 4 for the vertical crystal of Beam 1 at 6.8 TeV. The reference orientation was successfully identified for all four crystals both at injection and top energy, as shown in detail in Appendix A. The width of the channeling well is related to a quantity called *critical angle*, which defines the acceptance of the process and is calculated as:

$$\theta_c = \sqrt{\frac{2U_{max}}{pv}}\left(1 - \frac{R_c}{R}\right), \tag{1}$$

where U_{max} is the height of the potential well generated by neighboring crystalline planes, p and v are the momentum and speed of the incoming particle, R is the bending radius of the crystal and R_c is the *critical radius* of the crystal, a parameter that quantifies the maximum allowed bending radius over which the channeling process becomes impossible due to the deformation of the potential well. For the LHC case, the critical angle is of the order of 10 μ rad at 450 GeV and of the order of 2 μ rad at 6.8 TeV. Finally, the width of the full region with reduced signal of the crystal BLM is proportional to the bending angle of the crystal, validating this geometrical parameter.

In a *linear scan*, the crystal collimator is set at the previously identified optimal channeling orientation, while the jaw of the absorber that intercepts the deflected halo is retracted from the beam. In this condition, the halo is intercepted by the downstream collimators, which are kept at their nominal settings. The jaw is then progressively inserted back towards the beam, while losses at its location are continuously monitored. As the jaw starts intercepting the deflected halo, the corresponding BLM signal starts to increase until it reaches a certain plateau level. The scan is interrupted when the jaw touches the primary beam, as signaled by a massive spike in the BLM signal. By fitting the rise of the BLM signal with an error function, corresponding to the integral of the intercepted Gaussian beam coming out of the crystal, it is possible to estimate the displacement of the deflected beam with respect to the primary beam envelope. For the purpose of this analysis, the fitting function only accounts for the contribution of the Gaussian-shaped channeled beam, i.e. the initial rise of the integrated profile. Other contributions to the shape of the measured loss profile after the channeled beam has been fully integrated, due to other kinds of interaction processes with the crystal, are discussed in [28]. The displacement is then converted into a measurement of the bending angle θ via transfer functions describing the trajectory of the circulating particles:

$$\theta = \frac{\Delta z - n\sqrt{\epsilon\beta_2}(\cos\varphi_{21} - 1)}{\sqrt{\beta_1\beta_2}\sin\varphi_{21}}, \tag{2}$$

where Δz is the distance between the center of the deflected beam and the primary beam envelope measured at the location of the absorber, n is the distance of the crystal from the center of the beam (expressed

in units of beam r.m.s. size), ϵ is the beam emittance (the nominal normalized value of 3.5 μ m is assumed), β is the Twiss parameter related to the transverse size of the beam at the location of the crystal (1) and absorber (2), and φ_{21} is the phase advance between the two locations. The ratio between the signal recorded just before touching the primary beam and the plateau of the error function gives an estimate of the efficiency of the multiturn channeling process. An example is shown in Fig. 5. Linear scans were performed at injection and at top energy, as shown in detail in Appendix B. The measured bending angle and multiturn channeling efficiency are reported in Table 3. The uncertainty of these estimates is calculated as the propagation of the contributions due to the measured quantities, to the optical functions [32] and to the error function fit. The measured bending angle is compatible the specification of 50 ± 2.5 μ rad given to the manufacturers, resulting from detailed analytical studies as a trade-off between different requirements for operation at the LHC [33]. When compared to the X-ray results in Table 2, however, measurements at the LHC give a systematically slightly smaller value, although the difference is still within the uncertainty. The origin of this discrepancy is currently under investigation. The measured multiturn channeling efficiency is of the order of about 70% or higher in all cases, which is in line with expectations from previous measurements [29,34]. Given the complexity of the measurement and the varying data quality, reflected in the relatively large uncertainty, these estimates are to be considered as indicative figures. Due to the limited commissioning time with protons available in 2023, linear scans with the horizontal crystal on Beam 1 could only be performed at injection. However, a rough estimate of the bending angle at top energy can be extracted from the width of the angular scan profile, confirming measurements at injection. Furthermore, the performance in terms of channeling efficiency at injection is comparable to that of the horizontal crystal on Beam 2. In light of these observations, no issues are expected for the horizontal crystals at top energy, despite the lack of direct measurements.

5. Conclusions

At the beginning of Run 3 of the LHC, an extensive campaign of crystal collimation tests with proton beams was successfully carried out at injection and at at the unprecedented top energy of 6.8 TeV. This allowed the full characterization of the upgraded crystal collimator devices built for HL-LHC in preparation for long-term operation with heavy-ion beams. The orientation that maximizes the probability of the channeling process was successfully identified in all cases, while the measured bending angle and multiturn channeling efficiency were found to be well within expectations.

Declaration of competing interest

The authors declare that they have no known competing financial interests or personal relationships that could have appeared to influence the work reported in this paper.

Acknowledgments

Research on crystal collimation for the LHC is supported by the HL-LHC Project. The crystals installed in the LHC were manufactured by INFN-Ferrara and PNPI. The authors would like to thank the LHC engineers in charge and machine coordinators for their support.

Appendix A. Angular scans performed at injection and at top energy

Figs. A.6 and A.7 collect the angular scans performed for all crystals with proton beams at injection and top energy respectively. The plots show the BLM signal recorded at the location of the crystal during the rotation. The signal is normalized by the instantaneous rate of lost particles during the measurement, and then further normalized by the average level of the flat edges of the scan.

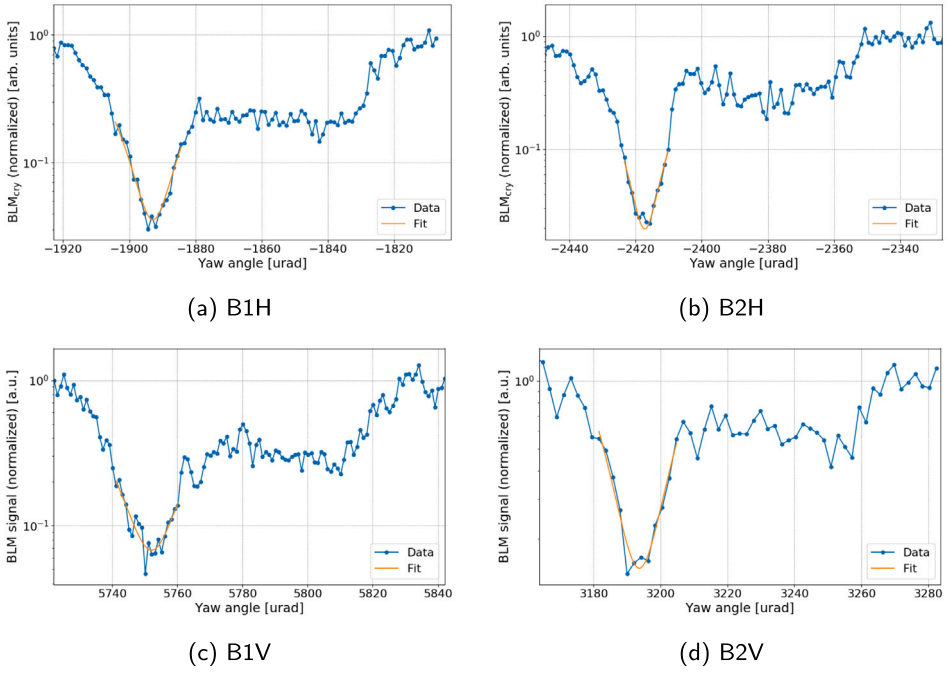

Fig. A.6. BLM signal at the crystal location recorded during angular scans performed for each crystal with protons at 450 GeV. The parabolic fit of the channeling dip is also shown.

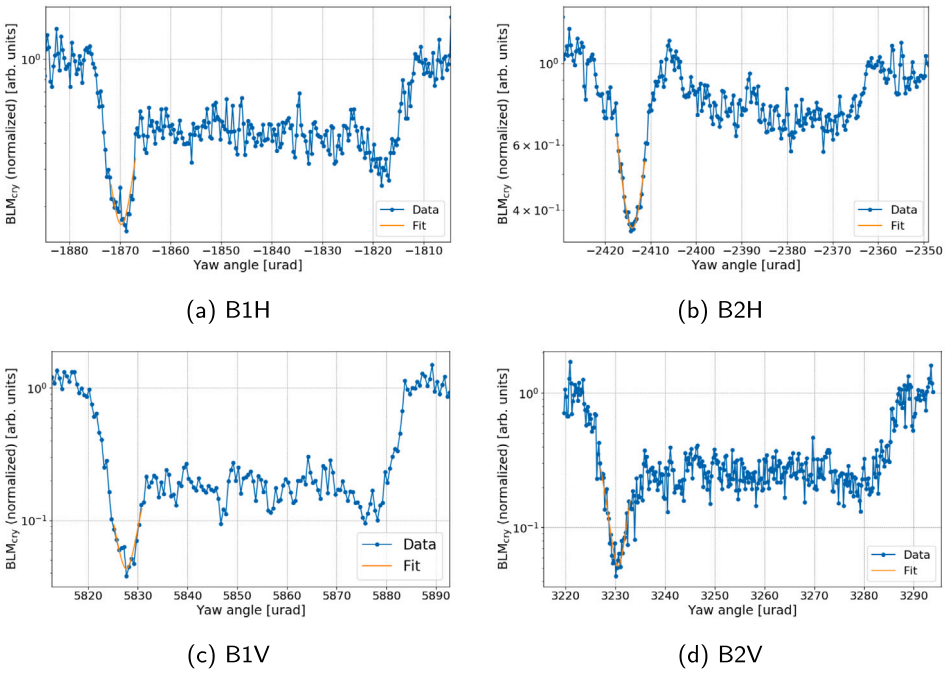

Fig. A.7. BLM signal at the crystal location recorded during angular scans performed for each crystal with protons at 6.8 TeV. The parabolic fit of the channeling dip is also shown.

Appendix B. Linear scans performed at injection and at top energy

Figs. B.8 and B.9 collect the linear scans performed for all crystals with proton beams at injection and top energy respectively. The plots show the BLM signal recorded at the location of the absorber during its progressive insertion. The signal is normalized by the instantaneous rate of lost particles during the measurement, and then further normalized by the saturation level of the losses recorded just before touching the primary beam. The jaw position is measured from the beam axis. Due to time constraints, this measurement could not be performed at top energy for the horizontal crystal of Beam 1.

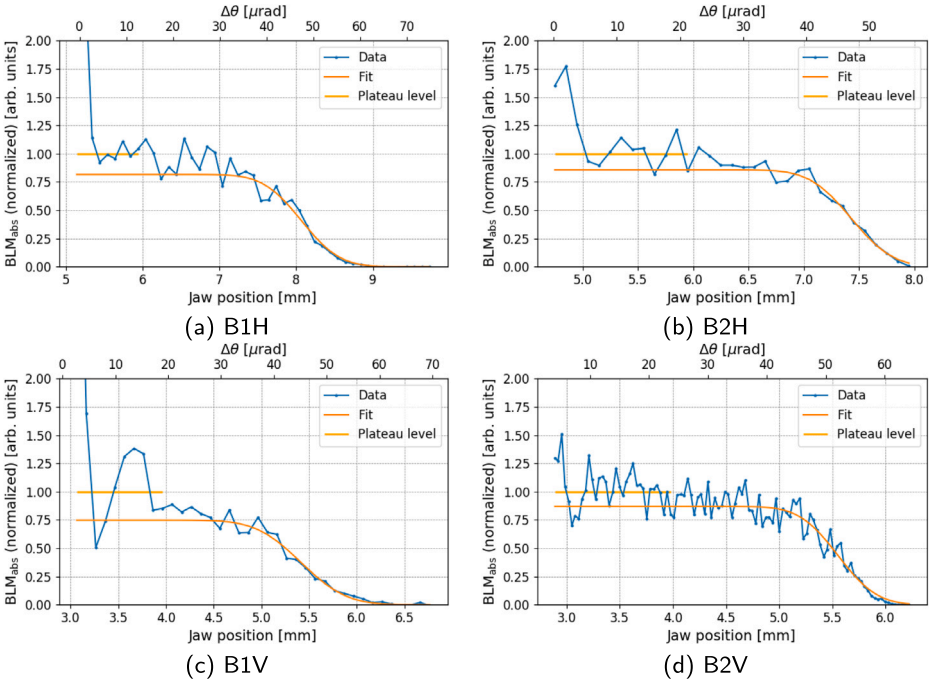

Fig. B.8. BLM signal at the absorber location during linear scans performed for each crystal with protons at 450 GeV. The error function fit of the signal profile is also shown.

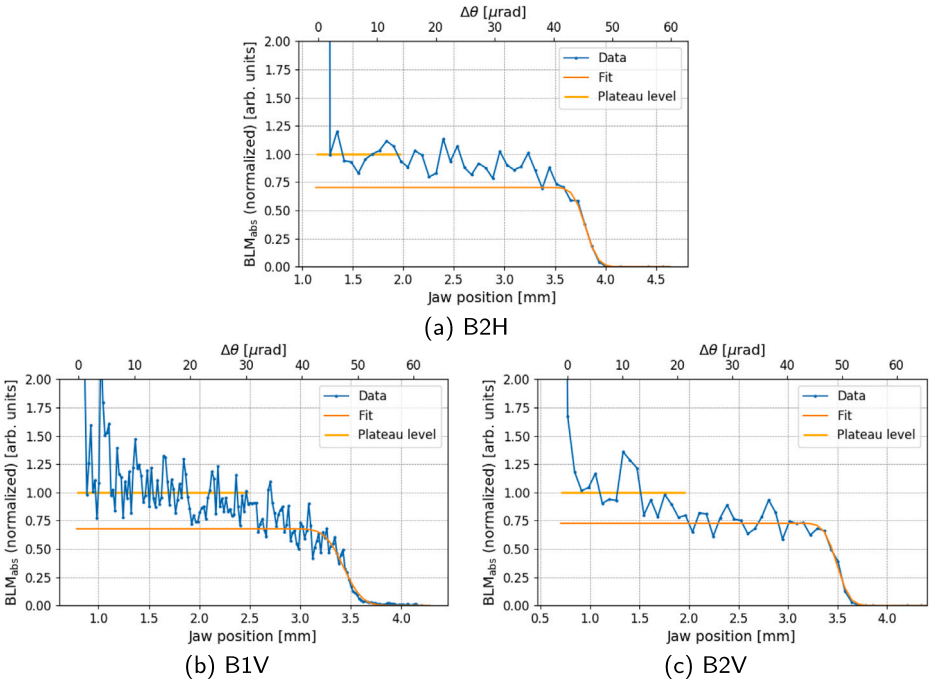

Fig. B.9. BLM signal at the absorber location during linear scans performed for each crystal with protons at 6.8 TeV. The error function fit of the signal profile is also shown.

References

[1] O.S. Bruning, P. Collier, P. Lebrun, S. Myers, R. Ostojic, J. Poole, P. Proudlock, LHC Design Report Vol. 1: The LHC Main Ring, 2004, http://dx.doi.org/10.5170/CERN-2004-003-V-1.

[2] R. Bruce, M. Jebramcik, J. Jowett, T. Mertens, M. Schaumann, Performance and luminosity models for heavy-ion operation at the CERN Large Hadron Collider, Eur. Phys. J. Plus 136 (2021) http://dx.doi.org/10.1140/epjp/s13360-021-01685-5.

[3] J. Coupard, et al., LHC Injectors Upgrade, Technical Design Report: v.2: Ions, 2016, http://dx.doi.org/10.17181/CERN.L6VM.UOMS.

[4] O. Brüning, L. Rossi, The High Luminosity Large Hadron Collider, World Scientific, 2015, http://dx.doi.org/10.1142/9581, arXiv:https://www.worldscientific.com/doi/pdf/10.1142/9581, URL https://www.worldscientific.com/doi/abs/10.1142/9581.

[5] I. Béjar Alonso, O. Brüning, P. Fessia, L. Rossi, L. Tavian, M. Zerlauth, High-Luminosity Large Hadron Collider (HL-LHC): Technical design report, 10, 2020, http://dx.doi.org/10.23731/CYRM-2020-0010.

[6] P. Hermes, R. Bruce, J. Jowett, S. Redaelli, B. Ferrando, G. Valentino, D. Wollmann, Measured and simulated heavy-ion beam loss patterns at the CERN Large Hadron Collider, Nucl. Instrum. Methods Phys. Res. A 819 (2016) 73–83, http://dx.doi.org/10.1016/j.nima.2016.02.050.

[7] S. Redaelli, R. Bruce, A. Lechner, A. Mereghetti, Chapter 5: Collimation system, CERN Yellow Rep. Monogr. 10 (2020) 87–114, http://dx.doi.org/10.23731/CYRM-2020-0010.87.

[8] H.H. Braun, A. Fassò, A. Ferrari, J.M. Jowett, P.R. Sala, G.I. Smirnov, Hadronic and electromagnetic fragmentation of ultrarelativistic heavy ions at LHC, Phys. Rev. ST Accel. Beams 17 (2014) 021006, http://dx.doi.org/10.1103/PhysRevSTAB.17.021006, URL https://link.aps.org/doi/10.1103/PhysRevSTAB.17.021006.

[9] R. Bruce, M. Di Castro, I. Lamas, S. Redaelli, Upgrade of the crystal collimation test stand in IR7, Tech. rep. LHC-TC-EC-0015, 2021.

[10] K. Elsener, G. Fidecaro, M. Gyr, et al., Proton extraction from the CERN SPS using bent silicon crystals, Nucl. Instrum. Methods Phys. Res. B 119 (1) (1996) 215–230, http://dx.doi.org/10.1016/0168-583X(96)00239-X, URL https://www.sciencedirect.com/science/article/pii/0168583X9600239X.

[11] A.G. Afonin, V.T. Baranov, V.M. Biryukov, et al., High-efficiency beam extraction and collimation using channeling in very short bent crystals, Phys. Rev. Lett. 87 (2001) 094802, http://dx.doi.org/10.1103/PhysRevLett.87.094802, URL https://link.aps.org/doi/10.1103/PhysRevLett.87.094802.

[12] W. Scandale, A.M. Taratin, Channeling and volume reflection of high-energy charged particles in short bent crystals. Crystal assisted collimation of the accelerator beam halo, Phys. Rep. 815 (2019) 1–107, http://dx.doi.org/10.1016/j.physrep.2019.04.003.

[13] W. Scandale, G. Arduini, M. Butcher, et al., Observation of channeling for 6500 GeV/c protons in the crystal assisted collimation setup for LHC, Phys. Lett. B 758 (2016) 129–133, http://dx.doi.org/10.1016/j.physletb.2016.05.004, URL https://www.sciencedirect.com/science/article/pii/S0370269316301514.

[14] S. Redaelli, M. Butcher, C. Barreto, et al., First observation of ion beam channeling in bent crystals at multi-TeV energies, Eur. Phys. J. C 81 (2021) http://dx.doi.org/10.1140/epjc/s10052-021-08927-x.

[15] W. Scandale, et al., UA9 Collaboration, Feasibility of crystal-assisted collimation in the CERN accelerator complex, Internat. J. Modern Phys. A 37 (13) (2022) 2230004, http://dx.doi.org/10.1142/S0217751X22300046.

[16] J. Lindhard, Influence of crystal lattice on motion of energetic charged particles, Kongel. Dan. Vidensk. Selsk., Mat.-Fys. Medd. 34 (14) (1965) URL https://www.osti.gov/biblio/4536390.

[17] V.M. Biryukov, Y.A. Chesnokov, V.I. Kotov, Crystal Channeling and Its Application at High-Energy Accelerators, Springer, 1997.

[18] C. Bahamonde, A. Lechner, R. Rossi, Crystal channeling of ions on different TCSG materials, 2018, presented at LHC Collimation Upgrade Specification Meeting.

[19] D. Quartullo, P. Arpaia, N. Biancacci, et al., Electromagnetic characterization of the crystal primary collimators for the HL-LHC, Nucl. Instrum. Methods Phys. Res. A 1010 (2021) 165465, http://dx.doi.org/10.1016/j.nima.2021.165465, URL https://www.sciencedirect.com/science/article/pii/S0168900221004502.

[20] S. Montesano, et al., Installation of the LUA9 equipment in IR7 of the LHC, Tech. rep. LHC-TEC-EC-0001, 2014.

[21] S. Redaelli, et al., Installation in IR7 of primary crystal collimators (TCPC) on beam 2, Tech. rep. LHC-TC-EC-0008, 2016.

[22] R. Bruce, D. Mirarchi, S. Redaelli, Functional and operational conditions of the crystal primary collimators, Tech. rep., 2019.

[23] M. D'Andrea, D. Mirarchi, S. Redaelli, Simulations of miscut effects on the efficiency of a crystal collimation system, in: 13th International Particle Accelerator Conference, 2022, http://dx.doi.org/10.18429/JACoW-IPAC2022-TUPOTK060.

[24] M. Pesaresi, W. Ferguson, J. Fulcher, G. Hall, M. Raymond, M. Ryan, O. Zorba, Design and performance of a high rate, high angular resolution beam telescope used for crystal channeling studies, J. Instrum. 6 (04) (2011) P04006.

[25] R. Rossi, L.S. Esposito, M. Pesaresi, G. Hall, W. Scandale, Track reconstruction and analysis of particle interactions in short bent crystals, JINST 18 (06) (2023) P06027, http://dx.doi.org/10.1088/1748-0221/18/06/P06027.

[26] R. Rossi, G. Cavoto, D. Mirarchi, S. Redaelli, W. Scandale, Measurements of coherent interactions of 400gev protons in silicon bent crystals, Nucl. Instrum. Methods Phys. Res. B 355 (2015) 369–373, http://dx.doi.org/10.1016/j.nimb.2015.03.001, Proceedings of the 6th International Conference Channeling 2014:"Charged & Neutral Particles Channeling Phenomena" October 5-10, 2014, Capri, Italy, URL https://www.sciencedirect.com/science/article/pii/S0168583X15002013.

[27] Malvern Panalytical Ltd, X'Pert – Thin film analysis XRD systems, 2023, URL https://www.malvernpanalytical.com/en/support/product-support/xpert3-range.

[28] V. Previtali, Performance evaluation of a crystal-enhanced collimation system for the LHC, 2010, Presented on 07 Oct 2010, URL https://cds.cern.ch/record/1302274.

[29] R. Rossi, Experimental assessment of crystal collimation at the Large Hadron Collider, 2017, Presented on 26 Jan 2018, URL https://cds.cern.ch/record/2644175.

[30] B. Dehning, E. Effinger, J. Emery, et al., The LHC Beam Loss Measurement System, 2007, pp. 4192–4194, http://dx.doi.org/10.1109/PAC.2007.4439980.

[31] G. Valentino, A.A. Nosych, R. Bruce, et al., Successive approximation algorithm for beam-position-monitor-based LHC collimator alignment, Phys. Rev. ST Accel. Beams 17 (2014) 021005, http://dx.doi.org/10.1103/PhysRevSTAB.17.021005, URL https://link.aps.org/doi/10.1103/PhysRevSTAB.17.021005.

[32] A. Wegscheider, A. Langner, R. Tomás, A. Franchi, Analytical N beam position monitor method, Phys. Rev. Accel. Beams 20 (2017) 111002, http://dx.doi.org/10.1103/PhysRevAccelBeams.20.111002, URL https://link.aps.org/doi/10.1103/PhysRevAccelBeams.20.111002.

[33] D. Mirarchi, G. Hall, S. Redaelli, W. Scandale, Design and implementation of a crystal collimation test stand at the Large Hadron Collider, Eur. Phys. J. C 77 (6) (2017) 424, http://dx.doi.org/10.1140/epjc/s10052-017-4985-4.

[34] M. D'Andrea, Applications of crystal collimation to the CERN large hadron collider (LHC) and its high luminosity upgrade project (HL-LHC), 2021, Presented on 23 Feb 2021, URL https://cds.cern.ch/record/2758839.